

Nonlinear analysis of free-electron-laser amplifiers with axial guide fields

H. P. Freund*

Naval Research Laboratory, Washington, D.C. 20375

(Received 21 September 1982)

The nonlinear evolution of free-electron lasers in the presence of an axial guide field is investigated numerically. A set of coupled nonlinear differential equations is derived which governs the self-consistent evolution of the wave fields and particle trajectories in an amplifier configuration. The nonlinear currents which mediate the interaction are computed by means of an average over particle phases, and the inclusion of fluctuating space-charge fields in the formulation permits the investigation of both the stimulated Raman and Compton scattering regimes. The initial conditions are chosen to describe the injection of a cold, axially propagating electron beam into the interaction region which consists of a uniform axial guide field and a helical wiggler field which increases to a constant level adiabatically over a distance of ten wiggler periods. After an initial transient phase, the results show a region of exponential growth of the radiation field which is in excellent agreement with linear theory. Saturation occurs by means of particle trapping. The efficiency of the interaction has been studied for a wide range of axial guide fields, and substantial enhancements have been found relative to the zero-guide-field limit.

I. INTRODUCTION

The use of axial guide magnetic fields in free-electron-laser (FEL) experiments has generally been restricted to low-energy (~ 1 MeV) and high-current (~ 1 kA) devices in which the axial field is necessary in order to confine the electron beam. As a consequence, a great deal of theoretical work has been devoted to the calculation of electron orbits,^{1,2} spontaneous radiation (i.e., noise) spectra,³ and the linear growth rate³⁻⁹ in the presence of an axial guide field. As shown in these works, a fortuitous consequence of the presence of the guide field is that both the noise spectrum and the linear growth rate are enhanced. Such enhancements are due to an increase in the transverse electron velocities and a decrease in the natural response frequency of the electrons. In the latter case, the natural frequency can become comparable to the frequency of the ponderomotive force which results from the beating of the radiation and wiggler fields. When this occurs the linear gain can become very large, and the interaction is analogous to that of driving an oscillator at its natural frequency. In view of the possible enhancements in the gain, the study of the nonlinear phase of the interaction assumes an added importance with a primary focus on possible enhancements in the saturation levels of the instability and the efficiency of the interaction.

The motivation for the present work is to investigate the effects of the guide field on the nonlinear regime of both the stimulated Raman and stimulated Compton scattering regimes of FEL operation. To this end, a set of coupled nonlinear differential equations is derived which describes the evolution of both particle orbits and the electrostatic and electromagnetic fields. The nonlinear currents which mediate the interaction are computed from the microscopic behavior of an ensemble of electrons by means of an average of the electron phases relative to the ponderomotive wave. This is equivalent to a time average over the electron orbits which, in turn, is equivalent to an ensemble average over the microscopic electron distribution. Thus although the macroscopic electron distribution does not explicitly appear, the formulation is equivalent to a fully kinetic treatment of the interaction and is capable of describing effects such as particle trapping in the ponderomotive wave. This is in contrast to the nonlinear analysis described recently by Friedland and Bernstein¹⁰ which is based on the cold-fluid model.

These equations are solved numerically for a configuration in which a uniform, monoenergetic electron beam is injected with purely axial velocities into the interaction region which consists of a uniform axial guide field and a helical wiggler field which increases adiabatically from zero in ten wiggler periods. The analysis is performed in one spatial di-

mension, although the electron trajectories are integrated for three dimensions in the velocity. In addition, since the problem of interest is that of an FEL amplifier, only a single electromagnetic and electrostatic wave is included corresponding to the choice of the fastest growing mode. Thus the analysis self-consistently describes the linear and nonlinear phases of the interaction of a uniform electron beam with a helical wiggler field in one dimension. The results of the simulation show, after an initial transient phase, a region of exponential growth of the radiation and space-charge fields which is in excellent agreement with the linear theory³⁻⁹ over the entire range of parameters studied. The onset of the nonlinear phase of the interaction appears quite suddenly, and saturation occurs by means of particle trapping. Most significantly, substantial enhancements in the interaction efficiency are found to occur.

The organization of the paper is as follows. The general equations are derived in Sec. II. Since the actual adiabatic entry of the electron beam into the wiggler is included in the analysis, we digress in Sec. III to describe the types of orbit which result in the absence of a radiation field. The numerical solutions to the complete set of coupled particle-field

equations are given in Sec. IV, and the conditions under which efficiency enhancements occur are described. A summary and discussion is given in Sec. V.

II. GENERAL EQUATIONS

The physical configuration we employ is one dimensional in that spatial variations are restricted to the z direction. The static magnetic field is taken to be of the form

$$\vec{B}(z) = B_0 \hat{e}_z + B_w(z) [\hat{e}_x \cos(k_w z) + \hat{e}_y \sin(k_w z)], \quad (1)$$

where B_0 and B_w are the amplitudes of the axial guide field and the wiggler field, respectively, k_w ($\equiv 2\pi/\lambda_w$, where λ_w is the wiggler period) denotes the wiggler wave vector, and it is assumed that $d \ln B_w / dz \ll k_w$. Thus we allow the wiggler amplitude to vary slowly in z while holding the period constant. In practice, we shall allow $B_w(z)$ to vary only over $0 < z < 10\lambda_w$, after which it shall be held constant, so that $d \ln B_w / dz \simeq 0.1 k_w$. The variable amplitudes and periods of the radiation and space-charge fields are included by means of the vector and scalar potentials

$$\delta \vec{A}(z, t) = \delta A(z) \left[\hat{e}_x \cos \left[\int_0^z dz' k_+(z') - \omega t \right] - \hat{e}_y \sin \left[\int_0^z dz' k_+(z') - \omega t \right] \right], \quad (2)$$

$$\delta \Phi(z, t) = \delta \Phi(z) \cos \left[\int_0^z dz' k(z') - \omega t \right], \quad (3)$$

where ω is the wave frequency, $\delta A(z)$ and $\delta \Phi(z)$ are the amplitudes of the vector and scalar potentials, and $k_+(z)$ and $k(z)$ are the wave vectors. Note that by the choice of parameters (i.e., primarily the pump strength, beam density, and axial field) the amplitudes and wave vectors will be slowly varying functions of z ; however, no such assumption is made *a priori*.

The microscopic current density can be written as the following sum over individual particle trajectories:

$$\delta \vec{J}(z, t) = -en_b \frac{L}{N_T} \sum_{i=1}^{N_T} \vec{v}_i(z, t_{i0}) \frac{\delta(t - \tau_i(z, t_{i0}))}{|v_{zi}(z, t_{i0})|}, \quad (4)$$

where N_T is the total number of electrons within the interaction region of length L , n_b is the average electron density, $\vec{v}_i(z, t_{i0})$ is the velocity of the i th electron at position z which entered the interaction region (i.e., crossed the $z=0$ plane) at time t_{i0} , and

$$\tau_i(z, t_{i0}) \equiv t_{i0} + \int_0^z \frac{dz'}{v_{zi}(z', t_{i0})}. \quad (5)$$

The system is assumed to be quasistatic (i.e., in a temporal steady state) so that particles which enter the interaction region at times t_0 separated by integral multiples of a wave period will execute identical orbits.¹¹ As a result $\vec{v}_i(z, t_{i0}) = \vec{v}_j(z, t_{j0})$, where $t_{i0} = t_{j0} + 2\pi N/\omega$ for integer N .

Substitution of the microscopic fields and current density into Maxwell's equation yields

$$\frac{d^2}{dz^2} \delta a + \left[\frac{\omega^2}{c^2} - k_+^2 \right] \delta a = \frac{\omega_b^2}{c^2} \frac{v_{z0}}{c} \left\langle \frac{v_1 \cos \psi - v_2 \sin \psi}{v_3} \right\rangle, \quad (6)$$

$$2k_+^{1/2} \frac{d}{dz} (k_+^{1/2} \delta a) = - \frac{\omega_b^2}{c^2} \frac{v_{z0}}{c} \left\langle \frac{v_1 \sin \psi + v_2 \cos \psi}{v_3} \right\rangle, \quad (7)$$

$$\left[\frac{d^2}{dz^2} - k^2 \right] \delta\phi = 2 \frac{\omega_b^2}{c^2} v_{z0} \left\langle \frac{\cos\psi_l}{v_3} \right\rangle, \quad (8)$$

$$2k^{1/2} \frac{d}{dz} (k^{1/2} \delta\phi) = -2 \frac{\omega_b^2}{c^2} v_{z0} \left\langle \frac{\sin\psi_l}{v_3} \right\rangle, \quad (9)$$

where an average over a wave period has been performed. In Eqs. (6)–(9), $\omega_b^2 \equiv 4\pi e^2 n_b/m$, v_{z0} is the initial axial velocity of the electrons, $\delta a \equiv e \delta A/mc^2$, $\delta\phi \equiv e \delta\Phi/mc^2$,

$$\psi \equiv \psi_0 + \int_0^z dz' (k_+ + k_w - \omega/v_3), \quad (10)$$

$$\psi_l \equiv \psi_0 + \int_0^z dz' (k - \omega/v_3), \quad (11)$$

$\psi_0 \equiv -\omega t_0$ is the initial phase, and (v_1, v_2, v_3) are the components of the electron velocity in the wiggler frame defined by the basis vectors $\hat{e}_1 = \hat{e}_x \cos(k_w z) + \hat{e}_y \sin(k_w z)$, $\hat{e}_2 = -\hat{e}_x \sin(k_w z) + \hat{e}_y \cos(k_w z)$, $\hat{e}_3 = \hat{e}_z$. Observe that it has been implicitly assumed that the electron beam is monoenergetic and that all electrons have the same initial axial velocity. In addition,

$$\langle \mathcal{F} \rangle \equiv \frac{1}{N_\omega} \sum_{i=1}^{N_\omega} \mathcal{F} \quad (12)$$

represents a phase average where N_ω denotes the number of electrons in a single wave period. Thus following Sprangle *et al.*¹¹ the quasistatic assumption has permitted the reduction of the problem to the consideration of the initial beam segments for which steady-state orbits of the beam electrons are described by particles which enter the wiggler region within a wave period. The actual length of these segments is $2\pi v_{z0}/\omega$ so that $N_\omega = 2\pi N_T v_{z0}/\omega L$. For sufficiently large N_ω , the discrete nature of the phase average (12) can be replaced by an integral over the initial phases ψ_0 as follows:

$$\langle \mathcal{F} \rangle = \frac{1}{2\pi} \int_{-\pi}^{\pi} d\psi_0 \mathcal{F}. \quad (13)$$

In this form the field equations are identical to those derived by Sprangle *et al.*¹¹

In order to complete the formulation, the electron orbit equations in the presence of the static and fluctuating fields must be specified. These equations are of the form

$$\frac{d}{dz} p_1 = - \left[\frac{\Omega_0}{\gamma} - k_w v_3 \right] \frac{p_2}{v_3} + mc \left[\left[\frac{\omega}{v_3} - k_+ \right] \delta a \sin\psi + \cos\psi \frac{d}{dz} \delta a \right], \quad (14)$$

$$\frac{d}{dz} p_2 = \left[\frac{\Omega_0}{\gamma} - k_w v_3 \right] \frac{p_1}{v_3} - m \Omega_w + mc \left[\left[\frac{\omega}{v_3} - k_+ \right] \delta a \cos\psi - \sin\psi \frac{d}{dz} \delta a \right], \quad (15)$$

where $p_{1,2} \equiv \gamma m v_{1,2}$, $\Omega_{0,w} \equiv |e B_{0,w}/mc|$, $\gamma \equiv (1 - v^2/c^2)^{-1/2}$,

$$\begin{aligned} \frac{d}{dz} v_3 &= \frac{\Omega_w}{\gamma} \frac{v_2}{v_3} + \frac{c}{v_3} \frac{\delta a}{\gamma} \left[k_+ - \omega \frac{v_3}{c^2} \right] (v_1 \sin\psi + v_2 \cos\psi) \\ &\quad - \frac{c}{\gamma v_3} \frac{d}{dz} \delta a (v_1 \cos\psi - v_2 \sin\psi) - \frac{c^2}{\gamma \gamma_z^2 v_3} \left[k \delta\phi \sin\psi_l - \cos\psi_l \frac{d}{dz} \delta\phi \right], \end{aligned} \quad (16)$$

and $\gamma_z^2 \equiv (1 - v_z^2/c^2)^{-1}$. Both the linear and nonlinear evolution of the FEL amplifier, therefore, are included in Eqs. (6)–(9) for the field quantities and (14)–(16) for the orbits of an ensemble of electrons having initial phases $-\pi \leq \psi_0 \leq \pi$.

III. SINGLE-PARTICLE ORBITS

Since an adiabatic entry region into the wiggler is included in the analysis, it is useful to consider the form which the single-particle orbits take as they emerge into the constant- B_w region as a function of B_0 . It should be remarked here that the radially

homogeneous wiggler under consideration is neither curl nor divergence free and is a reasonable approximation for a realizable wiggler field only as long as $k_w r \ll 1$ and $d \ln B_w(z)/dz \ll k_w$, where r measures the radial displacement of the electron trajectories from the axis of symmetry. The question we examine in this section, therefore, is the effect of the adiabatic increase in $B_w(z)$ on the trajectories of electrons which enter the wiggler with purely axial motion.

The appropriate equations of motion follow immediately from (14)–(16) in the absence of fluctuating fields,

$$\frac{d}{dz} v_1 = - \left[\frac{\Omega_0}{\gamma} - k_w v_3 \right] \frac{v_2}{v_3}, \quad (17)$$

$$\frac{d}{dz} v_2 = \left[\frac{\Omega_0}{\gamma} - k_w v_3 \right] \frac{v_1}{v_3} - \frac{\Omega_w}{\gamma}, \quad (18)$$

$$\frac{d}{dz} v_3 = - \frac{\Omega_w}{\gamma} \frac{v_2}{v_3}, \quad (19)$$

where γ is now a constant of the motion, and Ω_w is a function of z . The steady-state (or helical) orbits^{1,2} are obtained by requiring the derivatives to vanish in the constant- B_w region and results in solutions $v_1 = v_w \equiv \Omega_w v_{||} / (\Omega_0 - \gamma k_w v_{||})$, $v_2 = 0$, and $v_3 = v_{||}$, where $v_{||}$ is a constant determined by conservation of energy, i.e., $v_1^2 + v_{||}^2 = (1 - \gamma^{-2})c^2$. This equation is quartic in $v_{||}$ and describes at most four distinct classes of trajectory, of which one is characterized by motion antiparallel to \vec{B}_0 and will be ignored. Of the remaining three classes of trajectory, one is unstable. It is, therefore, difficult to propagate a coherent beam on these orbits, and it is of interest to determine whether, by adiabatic tapering of B_w , these orbits can be avoided. The three types of orbit propagating parallel to \vec{B}_0 are shown in Fig. 1, in which we plot $v_{||}$ vs $\Omega_0/\gamma k_w c$ (i.e., the axial field strength) for $\gamma = 3.5$ and $\Omega_w/\gamma k_w c = 0.05$. Observe that of the two classes of stable orbits, one is characterized by high axial velocities (denoted by group I) for low B_0 and decreases monotonically with the axial field up to a critical B_0 ($\Omega_0/\gamma k_w c \sim 0.76$ for the

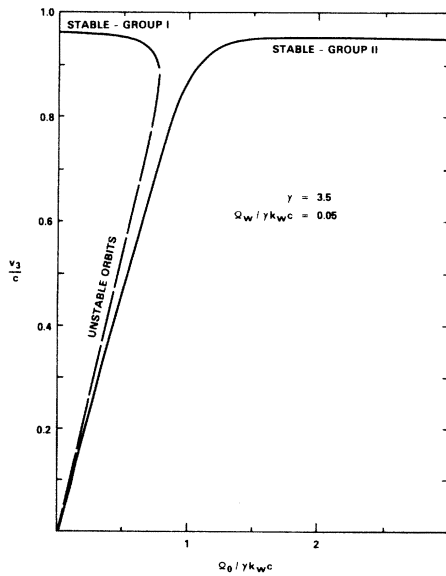


FIG. 1. Graph of the axial velocities corresponding to the steady-state trajectories as a function of the axial guide field.

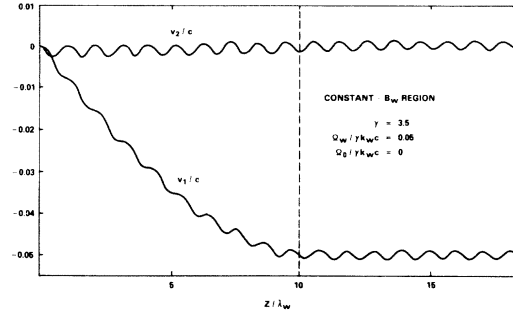


FIG. 2. Plot of the single-particle trajectories vs axial position of $\Omega_0/\gamma k_w c = 0.0$, $\Omega_w/\gamma k_w c = 0.05$, and $\gamma = 3.5$.

case illustrated) at which point there is a transition to the unstable orbits. The second class of stable trajectory (denoted by group II) is characterized by a monotonically increasing axial velocity with B_0 .

In the integration of the orbit equations it shall be assumed that

$$B_w(z) = \begin{cases} \frac{1}{2} B_w [1 - \cos(k_w z / 20)], & 0 \leq z \leq 10 \lambda_w \\ B_w, & z > 10 \lambda_w \end{cases} \quad (20)$$

which provides for a smooth, adiabatic transition to the constant- B_w region over ten wiggler periods. The results of the integration of the orbits with $B_w(z)$ characterized by (20) are shown in Figs. 2 and 3, where we plot the components of the velocity versus $k_w z$ for $\gamma = 3.5$ and $\Omega_w/\gamma k_w c = 0.05$. Note that the initial conditions on the velocity were chosen to be $v_1 = v_2 = 0$ and $v_3 = (1 - \gamma^{-2})^{1/2}c$. Figure 2 corresponds to parameters consistent with group-I steady-state orbits, and we find that the trajectories in the constant- B_w region differ only slightly from the steady-state case. As is evident in the figures, the bulk values for the magnitude of v_1 increase with the adiabatic rise in B_w , after which small oscillations about mean values corresponding

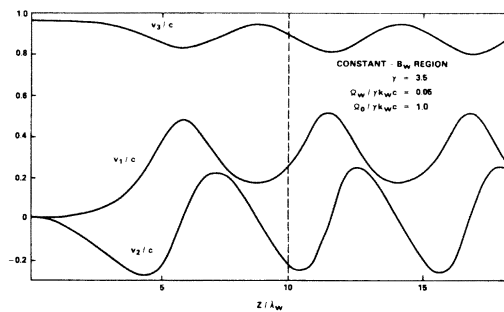


FIG. 3. Plot of the single-particle trajectories vs axial position for $\Omega_0/\gamma k_w c = 1.0$, $\Omega_w/\gamma k_w c = 0.05$, and $\gamma = 3.5$.

to the group-I trajectories are found in the constant- B_w region. Note that $\gamma k_w v_3 > \Omega_0$ for these orbits and, hence, $v_1 < 0$. In addition, $v_2 = 0$ for the steady-state orbits, and the electron trajectories in the constant- B_w region exhibit small oscillations about this value. The behavior of v_3 , while not shown explicitly, also exhibits small oscillations (of less than 1% of the mean value) about the appropriate value for the group-I orbit. Thus we conclude that it is possible to adiabatically inject electrons into the interaction region on near-steady-state orbits. However, it should be observed that as $\Omega_0/\gamma k_w c$ increases from 0 to 0.76 (corresponding to an increase in B_0), the magnitude of the fluctuation relative to the steady-state bulk value increases. This trend is characteristic of group-I-type injection and is indicative of the fact that it becomes increasingly difficult to obtain near-steady-state trajectories as the transition to orbital instability is approached, at which point ($\Omega_0/\gamma k_w c \simeq 0.76$) the orbits differ widely from the steady-state trajectories and exhibit large fluctuations in the velocity. As a result, it becomes impossible to either inject or propagate a coherent beam through the system.

Injection corresponding to near-steady-state orbits of the group-II type is illustrated in Fig. 3 for $\Omega_0/\gamma k_w c = 1.0$. Observe that $\gamma k_w v_3 < \Omega_0$ for these orbits and $v_1 > 0$ in this regime. Although orbital instability does not occur for group-II trajectories in one dimension, the orbits are characterized by low axial velocities for sufficiently small B_0 . As a consequence, it is possible for axially injected electrons with relativistic energies to be characterized by initial axial velocities much greater than that of the steady-state orbit. This is the case which corresponds to the orbit shown in Fig. 3, which is characteristic of the resulting trajectories for $\Omega_0/\gamma k_w c \leq 1$. The orbits in this regime may still be described as a perturbation about the steady-state orbits, but the perturbations are large. It is only when B_0 has increased along with the steady-state axial velocity that the perturbations about the helical orbits again become small (i.e., $\Omega_0/\gamma k_w c > 1.3$). As in the case of injection into near-group-I type of orbits in the vicinity of the orbital stability transition, large fluctuations in the equilibrium electron velocity results in a degradation of the FEL interaction.

In view of the preceding results regarding the adiabatic injection of relativistic electron beams into a combined axial guide field and helical wiggler field, we conclude that large-scale fluctuations in the electron velocity may be expected whenever $0.76 \leq \Omega_0/\gamma k_w c \leq 1.0$ for $\gamma = 3.5$ and $\Omega_w/\gamma k_w c = 0.5$. Within this range, the transverse components of the electron velocity may become sufficiently large that the radial excursions of the electron beam

make it difficult for the beam to propagate. In addition, the fluctuations in the axial velocity can cause a breakdown in the FEL wave particle resonance condition which, even if beam propagation is possible, will result in a substantial decrease in the gain.

IV. NUMERICAL SOLUTION

The set of coupled differential equations derived in Sec. II is solved numerically for an amplifier configuration in which a wave (ω, k_+) of arbitrary amplitude is injected into the system in concert with a monoenergetic electron beam. The initial conditions (at $z = 0$) imposed on the electron beam are chosen such that the particles are uniformly distributed in phase for $-\pi \leq \psi_0 \leq \pi$ in order to model the case of a continuous beam (i.e., the beam is not pre-bunched). Difficulties which arise from the inclusion of a necessarily finite number of electrons in the phase averages (12) were found to be overcome by the use of a Simpson's rule integrator for 61 particles per wave period. The use of larger numbers of electrons was found to result in discrepancies of considerably less than 1%. As in the integration of single-particle orbits in Sec. III, the wiggler field is assumed to increase adiabatically to a constant level over ten wiggler periods (20). The electromagnetic mode was chosen to correspond to the wave characterized by the highest linear growth rate. Thus if the equilibrium orbits are characterized by the steady-state trajectories described in Sec. III in the constant- B_w region, then the frequency and wave vector are determined by the intersection of the electrostatic beam mode

$$\omega = (k - \kappa)v_{||} \quad (21)$$

and the transverse electromagnetic mode

$$\omega^2 - k_+^2 c^2 - \frac{\omega_b^2 (\omega - k_+ v_{||})}{\gamma (\omega - \Omega_0/\gamma - k_+ v_{||})} = 0, \quad (22)$$

where

$$k = k_+ + k_w, \quad \kappa \equiv \omega_b \Phi^{1/2} / \gamma^{1/2} \gamma_z v_{||},$$

$$\Phi \equiv 1 - \frac{\Omega_0 \beta_w^2 \gamma_z^2}{(1 + \beta_w^2) \Omega_0 - \gamma k_w v_{||}}, \quad (23)$$

and $\beta_w \equiv v_w/v_{||}$. Finally, the initial level of fluctuations in the space-charge field is assumed to be zero.

Insofar as the electron orbits approximate the steady-state trajectories, it can be expected that the radiation field will experience a period of exponen-

tial growth (at a rate consistent with the linear theory) prior to saturation. As a consequence, a brief discussion of the linear dispersion equation is

$$[(\omega - kv_{\parallel})^2 - \kappa^2 v_{\parallel}^2](k - k_w - K_+)(k - k_w - K_-) \simeq \frac{1}{4} \beta_w^2 \xi^2 k_w^2 \frac{v_{\parallel}}{c} \frac{\omega}{Kc} [\omega \gamma_z^{-2} \Phi(\omega - \Omega_0/\gamma - k_+ v_{\parallel}) - \Omega_0(\omega - kv_{\parallel})/\gamma], \quad (24)$$

where $\xi \equiv \omega_b/\gamma^{1/2} k_w c$ is the beam strength parameter, $K^2 \equiv (\omega^2 - \omega_b^2/\gamma)/c^2$,

$$K_{\pm} \equiv \frac{1}{2} \left[K + \frac{\omega - \Omega_0/\gamma}{v_{\parallel}} \right] \pm \frac{1}{2} \left[(\Delta K)^2 + 2\xi^2 k_w^2 \frac{\Omega_0}{\gamma K v_{\parallel}} \right]^{1/2}, \quad (25)$$

and $\Delta K \equiv K - (\omega - \Omega_0/\gamma)/v_{\parallel}$. If the beam strength parameter is sufficiently small that $\xi \ll \gamma_z \times (B_w/B_0)^{2/3}$ and $\gamma(B_w/B_0)^{2/3} \Phi^{1/2}$, then (24) reduces still further to a more familiar cubic dispersion equation⁹

$$\delta k (\delta k + 2\kappa)(\delta k - \Delta k) \simeq -\frac{\beta_w^2}{4} \xi^2 k_w^2 \beta_{\parallel}^{-1} \Phi \frac{\omega}{\gamma_z^2 v_{\parallel}}, \quad (26)$$

where $\delta k \equiv k - \omega/v_{\parallel} - \kappa$, $\beta_{\parallel} \equiv v_{\parallel}/c$, and $\Delta k \equiv k_w + K - \omega/v_{\parallel} - \kappa$ is the frequency mismatch parameter.

The "strong-pump" (or Compton scattering) regime is obtained when $|\delta k| \gg |2\kappa|$. In this limit, (26) can be approximated as

$$(\delta k)^2 (\delta k - \Delta k) \simeq -\frac{\beta_w^2}{4} \xi^2 k_w^2 \beta_{\parallel}^{-1} \Phi \frac{\omega}{\gamma_z^2 v_{\parallel}}, \quad (27)$$

and peak growth occurs when $\Delta k \simeq 0$ at which point

$$(\delta k)_{\max} \simeq \frac{1}{2} (1 \pm i\sqrt{3}) \left(\frac{1}{2} \beta_w^2 \xi^2 \beta_{\parallel}^{-1} \Phi \right)^{1/3} k_w. \quad (28)$$

As a consequence, the requirement for Compton scattering to be valid becomes

$$\kappa \ll \frac{1}{16} \beta_w^2 \gamma_z^2 \beta_{\parallel} k_w. \quad (29)$$

The opposite (Raman scattering) regime occurs when $|2\kappa| \gg |\delta k|$, and (26) can be represented in the form

$$(\delta k)^2 - \Delta k \delta k + \frac{\beta_w^2}{4} \gamma_z^2 \beta_{\parallel} \kappa k_w \simeq 0. \quad (30)$$

Peak growth is again found for $\Delta k \simeq 0$, where

$$(\delta k)_{\max} \simeq \frac{1}{2} i \beta_w \gamma_z k_w (\beta_{\parallel} \kappa / k_w)^{1/2}. \quad (31)$$

of interest. The linear dispersion equation can be reduced to the following quartic equation in k_+ (> 0) (Ref. 9):

Therefore the Raman regime is found when

$$\kappa \gg \frac{1}{8} \beta_w^2 \gamma_z^2 \beta_{\parallel} k_w. \quad (32)$$

It should be observed that the criterion defining the Raman and Compton scattering regimes is dependent upon B_0 as well as on the beam and pump strengths. As a result, it is possible to make a transition from one to the other regime as a function solely of axial guide field. Since the principal objective of this paper is to examine the efficiency enhancement of an FEL amplifier in the presence of an axial guide field, the results of the simulation will be compared with the more complete form of the dispersion given by Eq. (24), and not by the idealized Raman and Compton regime approximations. It will be shown at a later stage of the discussion that the agreement between the linear theory as represented by Eq. (24) and the numerical simulation is excellent.

An example of the simulation results is shown in Fig. 4 in which the radiation-field amplitude $\delta a(z)$ and the growth rate $\Gamma(z)$ ($\equiv d \ln \delta a / dz$) are plotted as functions of axial position for $\Omega_0/\gamma k_w c = 0.0$

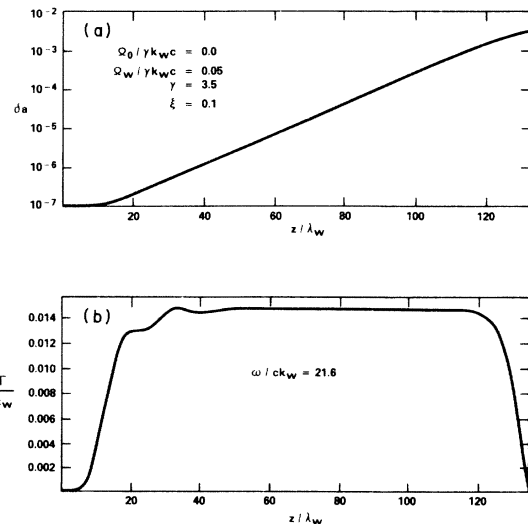


FIG. 4. Graphs of (a) the radiation-field strength and (b) growth rate, vs axial position for $\Omega_0/\gamma k_w c = 0.0$, $\Omega_w/\gamma k_w c = 0.05$, $\gamma = 3.5$, and $\xi = 0.1$.

(i.e., no axial guide field), $\Omega_w/\gamma k_w c = 0.05$, $\gamma = 3.5$, and $\delta a(z=0) = 10^{-7}$. As such, the illustrated calculation corresponds to the orbit calculation shown in Fig. 2. It is evident from the figure that, after an initial transient phase ($z/\lambda_w \leq 29.1$), an extended region of linear (or exponential) growth occurs as evidenced by the constancy of the growth rate. During this phase of the interaction, the growth rate as computed by the simulation is $\Gamma/k_w \simeq 0.0146$, which is in good agreement with the linear theory (24) which predicts a growth rate of $\Gamma_{\text{lin}}/k_w \simeq 0.0145$. Note that this corresponds to peak growth at a frequency $\omega/ck_w \simeq 21.6$.

Fluctuations in the growth rate found in the simulation are $\Delta\Gamma/k_w \simeq \pm 0.0002$, which is to be expected on the basis of the orbit calculation (Fig. 2) due to the relatively small fluctuation about the steady-state trajectory. Saturation begins to occur at $z/\lambda_w \simeq 114.1$, after which the growth rate rapidly decreases to zero at $z/\lambda_w \simeq 127.3$. At saturation, the radiation-field amplitude is $(\delta a)_{\text{sat}} \simeq 2.56 \times 10^{-3}$ which corresponds to an efficiency of 3.65%. Saturation occurs by means of particle trapping, and this will be discussed in detail later in this section.

As shown in Sec. II, increases in the axial guide field initially result in increasing fluctuations in the electron orbits about the steady-state trajectories. In addition, it has been shown that the linear growth rate also increases with B_0 for the group-I class of orbits.^{8,9} Therefore in order to determine the nonlinear effects the axial guide field and the adiabatic increase in the wiggler field, a series of calculations has been performed over a wide range of B_0 . The results of the simulation for $\Omega_0/\gamma k_w c = 0.5$ show the average growth rate during the linear phase of the interaction to be $\Gamma/k_w \simeq 0.030$ with a fluctuation of $\Delta\Gamma/k_w \simeq \pm 0.003$, which remains in good agreement with the linear-theory result (24) of $\Gamma_{\text{lin}}/k_w \simeq 0.029$. The increased growth rate leads to a decrease in the distance to saturation, which now occurs at $z_{\text{sat}}/\lambda_w \simeq 67.5$ at a field level of $(\delta a)_{\text{sat}} \simeq 3.30 \times 10^{-3}$. The wave frequency for this case (at peak growth) was $\omega/ck_w \simeq 19.4$, and the efficiency at saturation has increased to 4.92%. The decrease in frequency for this case resulted from a decrease in the axial velocity of the beam (see Fig. 1).

Increases in the axial guide field above this level (but still corresponding to group-I orbits) lead to larger fluctuations in both the orbits and the growth rate in the linear regime which culminates in a chaotic interaction at the transition to orbital instability at $\Omega_0/\gamma k_w c \simeq 0.76$. A transitional case is illustrated in Fig. 5 for which $\Omega_0/\gamma k_w c = 0.7$ and a frequency corresponding to peak growth of $\omega/ck_w \simeq 14.2$, in which the magnitude of the fluctu-

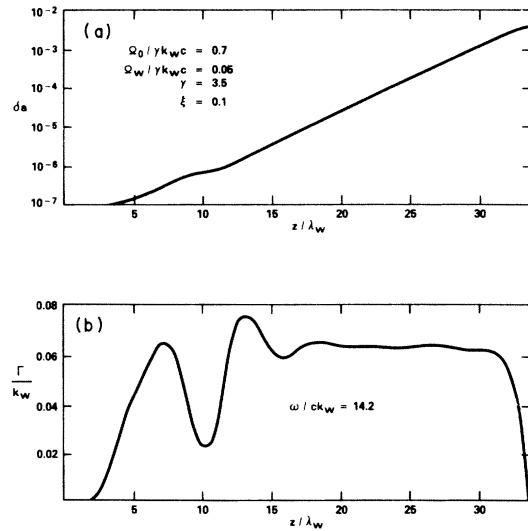


FIG. 5. Graphs of (a) the radiation-field strength and (b) growth rate, vs axial position for $\Omega_0/\gamma k_w c = 0.7$, $\Omega_w/\gamma k_w c = 0.05$, $\gamma = 3.5$, and $\xi = 0.1$.

tations in the growth rate is apparent. It should be noted, though, that for $20 \leq z/\lambda_w \leq 30$ the growth rate is relatively constant and has an average value of $\Gamma/k_w \simeq 0.063$, which is comparable to the result of the linear theory of $\Gamma_{\text{lin}}/k_w \simeq 0.060$. The increase in the growth rate results in a still further decline in the distance to saturation which now occurs at $z_{\text{sat}}/\lambda_w \simeq 32.6$; however, while $(\delta a)_{\text{sat}} \simeq 4.09 \times 10^{-3}$ represents a continuing increase in the radiation field, the efficiency at saturation has decreased to 4.02%. The decline in the efficiency is attributable to the decrease in the wave frequency.

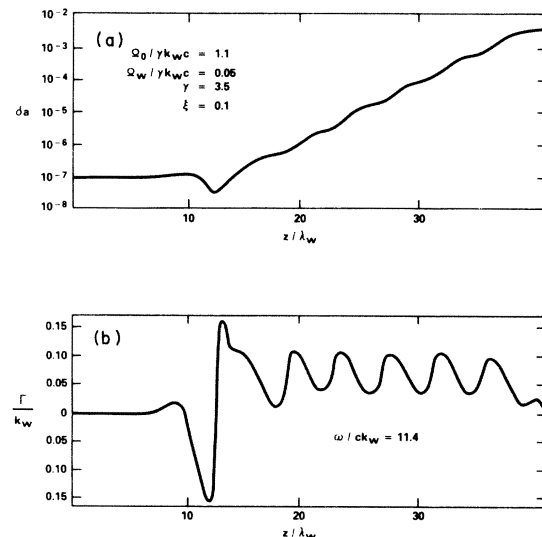


FIG. 6. Graphs of (a) the radiation-field strength and (b) growth rate, vs axial position for $\Omega_0/\gamma k_w c = 1.1$, $\Omega_w/\gamma k_w c = 0.06$, $\gamma = 3.5$, and $\xi = 0.1$.

For levels of B_0 such that $\Omega_0/\gamma k_w c > 0.76$ the electron trajectories correspond to perturbations about group-II-type orbits. However, as seen in Fig. 3, large divergences from the steady-state orbits occur for $\Omega_0/\gamma k_w c = 1.0$ and are characteristic of the low-bulk axial velocities in this regime. The implication of such orbit behavior is that since (1) the growth rate must also exhibit large-scale oscillations and (2) the resonant frequency is relatively low, the interaction efficiency can be expected to be small. Such an expectation is borne out by the simulation results as shown in Fig. 6 for $\Omega_0/\gamma k_w c \simeq 1.1$ and a frequency at peak growth of $\omega/c k_w = 11.4$. The system evidently shows the expected large-scale fluctuations in the growth rate ($\Delta\Gamma/k_w \simeq \pm 0.036$) about a mean value of $\Gamma/k_w \simeq 0.072$ after the transients have decayed ($z/\lambda_w \geq 20$). Note that the linear theory predicts a growth rate of $\Gamma_{\text{lin}}/k_w \simeq 0.056$ on the basis of the steady-state orbits, which is well within this range. Saturation occurs at $z_{\text{sat}}/\lambda_w \simeq 41.1$ for $(\delta a)_{\text{sat}} \simeq 4.91 \times 10^{-3}$; however, while the field amplitude is relatively high, the low frequency of the mode results in an efficiency of 3.88% which is comparable to the zero-axial-field limit. It should be remarked here that the case in which $\Omega_0/\gamma k_w c = 1.0$ (corresponding to Fig. 3) is not shown here since it represents a still more extreme example of the results of the large oscillations in the single-particle orbits and has a still lower efficiency.

Further increases in the axial guide field correspond with increases in the resonant frequency and decreases in the departure from the steady-state single-particle trajectories. As a consequence, the evolution of the radiation fields becomes more regular as well. For $\Omega_0/\gamma k_w c = 1.5$ and a frequency at peak growth of $\omega/c k_w = 20.3$, the simulation gives $\Gamma/k_w \simeq 0.021$ with a variation in the growth rate of less than 1%. It should be noted here that we also recover a growth rate of $\Gamma_{\text{lin}}/k_w \simeq 0.021$ from the linear theory (24). Saturation occurs at $z_{\text{sat}}/\lambda_w = 93.1$ for a field level of $(\delta a)_{\text{sat}} \simeq 3.19 \times 10^{-3}$ and an efficiency of 5.02%.

A summary of the frequencies and growth rates for the various simulations is given in Fig. 7 in which we plot $\omega/c k_w$ and Γ/k_w vs $\Omega_0/\gamma k_w c$. The curves for the frequency represent the variation in the resonant frequency at peak growth found from the intersection of the dispersion relations in Eqs. (21) and (22) for the appropriate value of v_{\parallel} from the steady-state trajectory. These values represent the frequencies used in the simulations. The solid line in the plot of Γ/k_w represents the results of the linear theory (24), again, for the appropriate steady-state trajectory while circles are used to denote the results found from the simulation in the linear re-

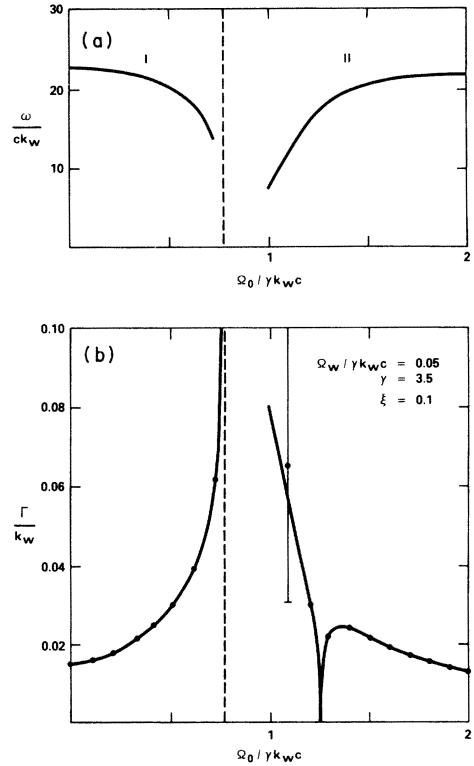


FIG. 7. Plots of (a) the peak growth rate and (b) the corresponding resonant frequency, vs axial field strength. Circles indicate the growth rates obtained from the numerical simulation.

gime. As seen in the figure, the agreement between the simulation and the linear theory is excellent. For the cases shown, it is only when $\Omega_0/\gamma k_w c = 1.1$ that the growth rates differ by more than about 2%, and this is due to the relatively large divergence of the single-particle orbits from the steady state. However, this problem no longer appears for $\Omega_0/\gamma k_w c = 1.2$, and we conclude that (for the parameters under study) difficulties resulting from nonsteady-state single-particle orbits are important only for $0.76 \leq \Omega_0/\gamma k_w c \leq 1.1$, where both the frequency and efficiency are low. Consequently, this regime will be ignored in the discussion of the overall radiation efficiency and saturation mechanism.

The energy-conversion efficiency and the distance to saturation are shown in Fig. 8 as functions of the axial magnetic field. The efficiency is defined to be the ratio of the total energy lost by the electrons through the interaction to the initial energy and may be shown by computation of the Poynting flux to be

$$\eta \simeq \frac{1}{\xi^2 \gamma (\gamma - 1) \beta_{\parallel}} \left[\frac{\omega}{c k_w} (\delta a)_{\text{sat}} \right]^2. \quad (33)$$

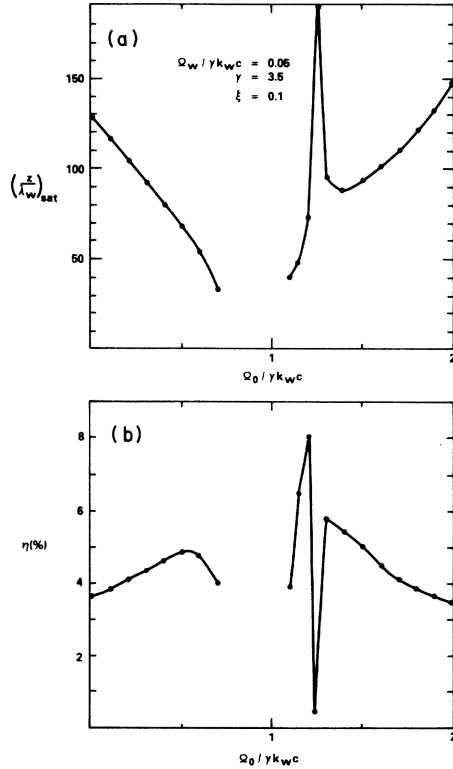


FIG. 8. Graphs of (a) the distance to saturation and (b) saturation efficiency, vs axial field strength.

It is evident from the figure that substantial enhancements of the efficiency are possible over that found in the absence of an axial guide field. For parameters corresponding to the group-I orbits, the peak efficiency is approximately 5% and occurs at $\Omega_0/\gamma k_w c \simeq 0.5$ for the chosen parameters and constitutes a 37% enhancement over the efficiency found

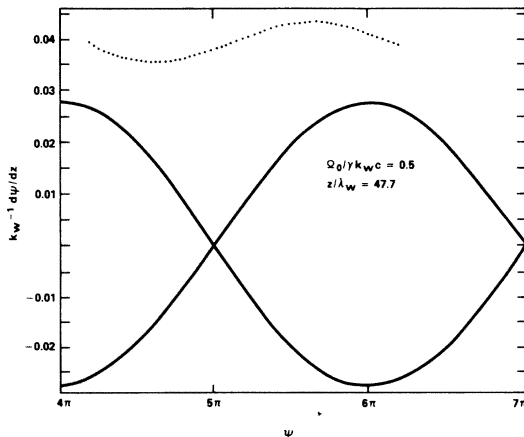


FIG. 9. Plot of the phase-space distribution for $\Omega_0/\gamma k_w c = 0.5$ and $z/\lambda_w = 47.7$ in the linear regime.

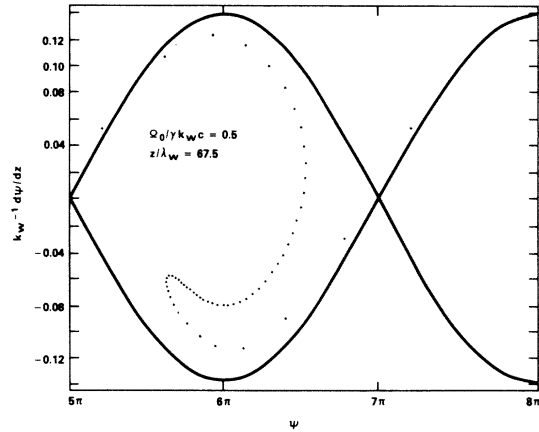


FIG. 10. Graph of the phase-space distribution for $\Omega_0/\gamma k_w c = 0.5$ and $z/\lambda_w = 67.5$ at saturation.

when no guide field is present. Note also that saturation occurs over a much shorter interaction length. However, the greatest enhancements in the efficiency are found for the group-II class of trajectories, for which a peak efficiency of approximately 8.09% is found for $\Omega_0/\gamma k_w c \simeq 1.2$ and corresponds to an efficiency enhancement of 122% relative to the $B_0 \rightarrow 0$ limit. It is important to bear in mind, however, that these enhancements in the efficiency occur at the expense of decreases in the resonant frequency of the interaction (see Fig. 7). Finally, the low efficiency found for $\Omega_0/\gamma k_w c \simeq 1.25$ corresponds to parameters for which $|\Phi| \ll 1$. In this regime (which is discussed in detail in Refs. 3 and 9) the ponderomotive potential and, hence, the linear growth rate vanish (Fig. 7).

As mentioned previously, saturation occurs by means of particle trapping in the ponderomotive potential which results from the beating of the wiggler and radiation fields. An example of this is shown in Figs. 9 and 10 in which the positions of the particles (represented by the dots) in phase space ($\psi, d\psi/dz$) are plotted for $\Omega_0/\gamma k_w c \simeq 0.5$ (i.e., group-I type of orbits) and $z/\lambda_w = 47.7$ and 67.5 , respectively. The solid lines in the figures represent the separatrix which encloses trapped (i.e., bounded) phase-space trajectories. It should be noted, however, that while the positions of the particles represent the results of the simulation, the separatrix represents an approximation as it is derived from a perturbation about the exact steady-state orbits described in Sec. II. As such the separatrix is strictly valid only insofar as the particle velocities are close to those for the helical trajectories, for which¹²

$$\frac{d^2}{dz^2} \psi = \frac{c^2(k + k_w)^4}{\gamma \gamma_z^2 \omega^2} \frac{v_w}{c} \Phi \delta a \sin \psi. \quad (34)$$

The separatrix, therefore, is given by

$$\frac{d}{dz}\psi = \pm 2 \frac{c(k+k_w)^2}{\gamma_z \omega} \left(\frac{v_w}{\gamma c} \Phi \delta a \right)^{1/2} \sin \left(\frac{\psi}{2} \right), \quad (35)$$

when $v_w \Phi > 0$, and

$$\frac{d}{dz}\psi = \pm 2 \frac{c(k+k_w)^2}{\gamma_z \omega} \left| \frac{v_w}{\gamma c} \Phi \delta a \right|^{1/2} \cos \left(\frac{\psi}{2} \right), \quad (36)$$

when $v_w \Phi < 0$. Because of this, the phase-space evolution of the particle distribution is dependent upon the signs of both v_w and Φ . For the group-I class of orbits (which includes the zero-guide-field limit) $v_w < 0$ and $\Phi > 0$ and the separatrix is determined by Eq. (36). However, the situation is more complicated for the group-II class of trajectories. In this case, while $v_w > 0$ for all the trajectories, Φ is less than zero for $\Omega_0/\gamma k_w c \leq 1.25$ (for the parameters chosen), and greater than zero for axial field strengths above this critical value. Thus one must distinguish between these two regimes in the analysis of the phase-space structure of the interaction. Since the single-particle trajectories are seen to be close to the steady-state orbits, it is expected that the separatrix shown in the figures [given by Eq. (36)] is a reasonable approximation.

The initial phase-space electron distribution (at $z=0$) is uniform in that $d\psi/dz = k+k_w - \omega/v_{z0}$ over $-\pi \leq \psi \leq \pi$ for all the particles. Figure 9 represents the phase-space distribution at a relatively late point in the linear phase of the interaction. It is evident, therefore, that the phase-space bunching of the particles has begun but that the trapping of the electrons has not yet occurred as the trajectories

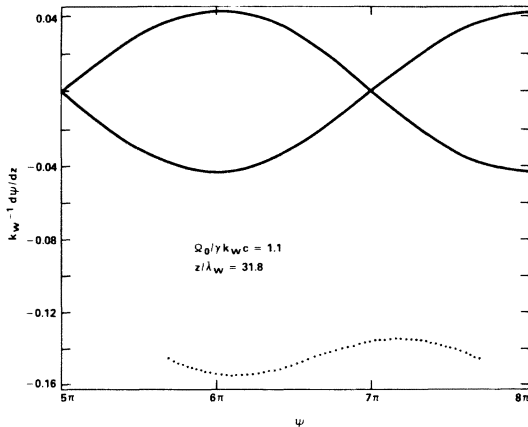


FIG. 11. Plot of the phase-space distribution for $\Omega_0/\gamma k_w c = 1.1$ and $z/\lambda_w = 31.8$ in the linear regime.

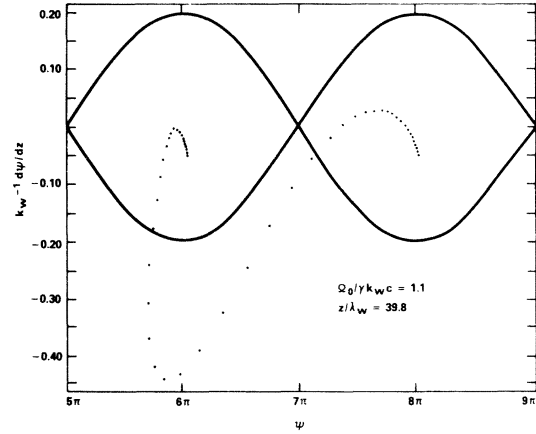


FIG. 12. Graph of the phase-space distribution for $\Omega_0/\gamma k_w c = 1.1$ and $z/\lambda_w = 39.8$ at saturation.

remain unbounded. In contrast, Fig. 10 represents the phase-space distribution at saturation, and it is clear that while two particles remain on unbounded orbits outside the separatrix, the bulk of the electrons has been trapped. The results shown here are in agreement with those found by Sprangle *et al.*¹¹

It was pointed out previously that the phase-space behavior of the electron beam is somewhat different when $\Phi < 0$. This discrepancy arises from the fact that the electron velocity is greater than the phase velocity of the ponderomotive wave [equal to $\omega/(k_+ + k_w)$] at peak growth ($d\psi/dz > 0$) when $\Phi > 0$, but less than the phase velocity of the ponderomotive wave when $\Phi < 0$. This can be illustrated by consideration of the small-signal gain in the single-particle regime,^{3,12}

$$G_L = \frac{\beta_w^2 \xi^2}{16\beta_{||}^2} L^3 k_w^2 k \Phi \frac{d}{d\theta} \left[\frac{\sin\theta}{\theta} \right]^2, \quad (37)$$

where $\theta = -\frac{1}{2}L d\psi/dz$. Therefore when $\Phi > 0$ peak gain occurs for $\theta \simeq -1.3$ and $d\psi/dz > 0$. However, in the opposite case when $\Phi < 0$, the peak gain occurs at $\theta \simeq 1.3$ and $d\psi/dz < 0$. This type of phase-space behavior is, indeed, found in the simulation and is evident in Figs. 11 and 12 in which we plot the phase-space distributions for $\Omega_0/\gamma k_w c = 1.1$ and $z/\lambda_w = 31.8$ (in the linear regime) and $z/\lambda_w = 39.8$ (at saturation). The separatrix in these figures was calculated from Eq. (36). Note that while the bulk of the particles is trapped on bounded phase-space trajectories at saturation (and that extreme phase bunching has occurred), a greater proportion of the particles appears to be outside the separatrix on unbounded orbits than in the other cases shown. However, this observation must be made in view of the fact that the single-particle orbits resemble those shown in Fig. 3, and the orbits

are widely divergent from the steady-state case. Thus the separatrix is difficult to determine precisely, and may differ greatly from that shown.

V. SUMMARY AND DISCUSSION

The principal objective of the study described in this paper is to examine the effect of an axial guide field on the nonlinear stage of the FEL interaction. Previous studies of the linear regime³⁻⁹ have revealed that large enhancements in the growth rate are possible, and the primary focus of this work is directed toward the question of whether enhancements in the nonlinear efficiency are possible as well. To this end, a self-consistent set of field and particle orbit equations is derived for a FEL amplifier which describes the evolution of both the wave amplitudes and trajectories for an ensemble of particles. It is important to observe that although no particle distribution function is explicitly included in the analysis, the source currents used in Maxwell's equations constitute time averages over the microscopic electron currents, and the level of the formulation is kinetic. The equations are then integrated numerically as functions of axial position subject to initial conditions which describe the interaction of a uniform electron beam with the guide and wiggler system. In fact, entry of the beam into the interaction region is effected by means of an adiabatically increasing wiggler amplitude which reaches a constant level after ten wiggler periods. Finally, inclusion of fluctuating space-charge fields in the formulation permits analysis of both the single-particle (Compton) and collective (Raman) regimes of operation.

The effect of the initial adiabatic increase of the wiggler field on the single-particle orbits was considered by numerical integration of the orbit equations in the absence of electromagnetic and electrostatic fields. The purpose of this phase of the analysis is the determination of the types of orbit which result; in particular, whether the electron orbits resemble the steady-state (helical) trajectories upon which the linear theories of the interaction are based. As such, the question of the relevance of the linear theories to both the simulation and to actual experiments¹³ is addressed. On the basis of this

work it was concluded that, for the configuration used, the electron orbits deviate only slightly from the helical trajectories except when $\Omega_0 \sim \gamma k_w c$, where the orbits are seen to execute large-scale oscillations about the steady-state trajectories. As a result, the linear theories are expected to be relevant over a wide range of parameters.

In fact, the numerical integration of the coupled particle-field equations bears out this conjecture. The results shown in Figs. 4-6 show that (except when $\Omega_0 \sim \gamma k_w c$), after an initial transient phase, an extended region of linear (i.e., exponential) growth occurs with growth rates which are in excellent agreement with the linear theory (see Fig. 7). Even in cases where substantial deviations from the steady-state trajectories occur, the growth rate is seen to oscillate about the predicted linear result (Fig. 6). Saturation is found to occur by means of particle trapping in the ponderomotive potential, and substantial enhancements of more than 100% are observed over the efficiency in the absence of an axial guide field. The greatest enhancements occur for parameters consistent with the group-II type of orbit and relatively large axial guide fields ($\Omega_0 \sim 1.2\gamma k_w c$) which is consistent with the results found in the experiment at the Naval Research Laboratory using the VEBA accelerator.¹³ It should be noted, however, that such enhancements in the efficiency correspond to decreases in the axial velocity of the electrons (and to increases in the transverse velocity) due to the presence of the axial guide field and, therefore, also correspond to decreases in the resonant frequency of the interaction.

Finally, it should also be remarked that these results have been obtained for a monoenergetic electron beam. Introduction of a finite energy spread can have important consequences on the growth rates and saturation levels. In fact, recent results¹⁴ using a full-scale particle simulation indicate that decreases in the efficiency are to be expected when a finite energy spread occurs.

ACKNOWLEDGMENTS

This work was supported under NAVSEA Contract No. SF68-342-602. The author would like to thank Dr. P. Sprangle, Dr. C. M. Tang, and Dr. I. B. Bernstein for helpful and stimulating discussions.

*Permanent address: Science Applications, Inc., 1710 Goodridge Drive, P.O. Box 1303, McLean, VA 22102.

¹L. Friedland, Phys. Fluids **23**, 2376 (1980).

²H. P. Freund and A. T. Drobot, Phys. Fluids **25**, 736 (1982).

³H. P. Freund, P. Sprangle, D. Dillenburg, E. H. da Jornada, B. Liberman, and R. S. Schneider, Phys. Rev. A **24**, 1965 (1981).

⁴P. Sprangle, V. L. Granatstein, and L. Baker, Phys. Rev. A **12**, 1697 (1975).

- ⁵T. Kwan and J. M. Dawson, *Phys. Fluids* 22, 1089 (1979).
- ⁶L. Friedland and J. L. Hirshfield, *Phys. Rev. Lett.* 44, 1456 (1980).
- ⁷I. B. Bernstein and L. Friedland, *Phys. Rev. A* 23, 816 (1981).
- ⁸L. Friedland and A. Fruchtman, *Phys. Rev. A* 25, 2693 (1982).
- ⁹H. P. Freund, P. Sprangle, D. Dillenburg, E. H. da Jornada, R. S. Schneider, and B. Liberman, *Phys. Rev. A* 26, 2004 (1982).
- ¹⁰L. Friedland and I. B. Bernstein, *Phys. Rev. A* 26, 2778 (1982).
- ¹¹P. Sprangle, C. M. Tang, and W. M. Manheimer, *Phys. Rev. A* 21, 302 (1980).
- ¹²S. H. Gold, R. H. Jackson, R. K. Parker, H. P. Freund, V. L. Granatstein, P. C. Efthimion, M. Herndon, and A. K. Kinkead, in *Physics of Quantum Electronics: Free-Electron Generators of Coherent Radiation*, edited by S. F. Jacobs, G. T. Moore, H. S. Pilloff, M. Sargent, M. O. Scully, and R. Spitzer (Addison-Wesley, Reading, Mass., 1982), Vol. 9, p. 741.
- ¹³R. K. Parker, R. H. Jackson, S. H. Gold, H. P. Freund, V. L. Granatstein, P. C. Efthimion, M. Herndon, and A. K. Kinkead, *Phys. Rev. Lett.* 48, 238 (1982).
- ¹⁴T. J. T. Kwan and C. M. Snell (unpublished).